Earth and Planetary Science Letters 583 (2022) 117441

Contents lists available at ScienceDirect

Earth and Planetary Science Letters

www.elsevier.com/locate/epsl

Aluminum and hydrogen partitioning between bridgmanite and high-pressure hydrous phases: Implications for water storage in the lower mantle

Takayuki Ishii [a,b,*], Eiji Ohtani [c], Anton Shatskiy [d]

[a] Center for High Pressure Science and Technology Advanced Research, Beijing, 100094, China
[b] Bayerisches Geoinstitut, University of Bayreuth, Universitätsstraße 30, 95447 Bayreuth, Germany
[c] Department of Earth Sciences, Graduate School of Science, Tohoku University, Sendai, Miyagi 980-8578, Japan
[d] Sobolev Institute of Geology and Mineralogy, Siberian Branch of Russian Academy of Sciences, 630090 Novosibirsk, Russia

ARTICLE INFO

Article history:
Received 15 September 2021
Received in revised form 20 January 2022
Accepted 14 February 2022
Available online 25 February 2022
Editor: J. Badro

Keywords:
bridgmanite
hydrous phase δ
hydrous phase H
hydrous phase D
phase relations
lower mantle

ABSTRACT

We clarified the phase relations of $MgSiO_3$-Al_2O_3-H_2O system under the uppermost lower-mantle conditions and the partitioning of aluminum and hydrogen between bridgmanite and hydrous minerals of hydrous phase δ-H solid solution and aluminous hydrous phase D. Bridgmanite coexists with hydrous phase D and δ-H at 25-28 GPa and 1000-1100 °C. Hydrous phase D becomes unstable above 1200 °C, while hydrous phase δ-H remains up to 1400 °C in the pressure range. Aluminum is strongly partitioned to both aluminous phases D and δ-H resulting in alumina depletion in bridgmanite. Fourier transform infrared spectroscopy indicates that bridgmanite contains undetectable water when coexisting with these hydrous phases, showing strong hydrogen partitioning into hydrous phases, such as phases D and δ-H. The depletion of alumina in bridgmanite modified the phase relations significantly in hydrated slabs descending into the lower mantle, i.e., the pressures of the garnet-bridgmanite and post-perovskite transformations are lowered under the wet conditions where these hydrous phases coexist. The dry nature of bridgmanite coexisting with hydrous phases suggests that the major water carriers in the lower mantle are hydrous phases. Bridgmanite cannot be the water reservoir at least in the upper part of the lower mantle and could provide dry rheology of the wet slabs in the lower mantle.

1. Introduction

Water can be transported into the deep upper mantle by slab subduction. It has been clarified that the mantle transition zone is considered to be a major water reservoir in the Earth (e.g., Utada et al., 2009; Karato, 2011; Yoshino and Katsura, 2013; Fei et al., 2017; Freitas et al., 2017; Wang et al., 2018). Recent discoveries of hydrous minerals in diamond such as phase egg and hydrous phase B together with hydrous ringwoodite also support existence of the wet mantle transition zone (Wirth et al., 2007; Pearson et al., 2014; Tschauner et al., 2018).

On the other hand, water transport and its distribution in the lower mantle is poorly known. Subducting slabs are descending into the lower mantle in subduction zones beneath North, Central, and South America, whereas stagnant slabs have been observed around the 660-km discontinuity beneath Japan and northeast China. Subduction of slabs into the lower mantle together with the collapse of the stagnant slabs further transports water into the lower mantle (Ohtani, 2005; Fukao and Obayashi, 2013). Recent seismological studies indicated that the top of the lower mantle is a region of low velocity and low Q anomalies (Lawrence and Wysession, 2006). Dehydration or existence of hydrous phases might cause such anomalies (Schmandt et al., 2014).

Experimental studies showed that hydrous δ-AlOOH is stable down to the bottom of the lower mantle and can affect physical properties of lower mantle rocks such as elasticity and thermal conductivity (Sano et al., 2008; Duan et al., 2018; Hsieh et al., 2020; Satta et al., 2021). On the other hand, dense hydrous magnesium silicates, such as superhydrous phase B ($Mg_{12}Si_3O_{12}(OH)_4$) and hydrous phase D (nominally $MgSi_2O_4(OH)_{12}$), are the major hydrous phases in the uppermost lower mantle. Recently discovered hydrous phase H, $MgSiO_4H_2$, is stable to 60 GPa and temperatures below 1300 °C (e.g. Nishi et al., 2014; Ohtani et al., 2014). This phase has an orthorhombic symmetry with the space group *Pnnm*, which is the same as that of δ-AlOOH at pressures above 10 GPa (Bindi et al., 2014; Sano-Furukawa et al., 2018), resulting

* Corresponding author at: Center for High Pressure Science and Technology Advanced Research, Beijing, 100094, China.
E-mail address: takayuki.ishii@hpstar.ac.cn (T. Ishii).

https://doi.org/10.1016/j.epsl.2022.117441
0012-821X/

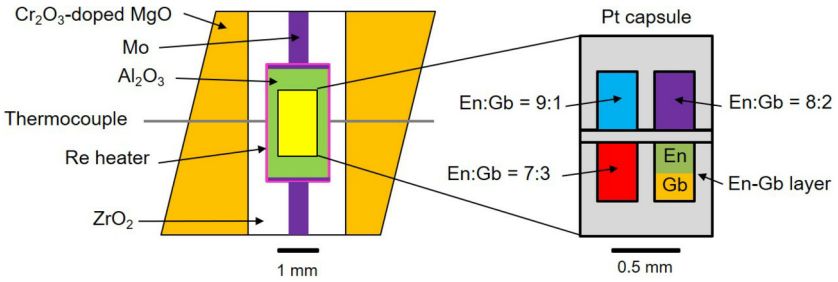

Fig. 1. The details of the cell assembly for this work. En, $MgSiO_3$ enstatite; Gb, $Al(OH)_3$ gibbsite.

Table 1
The starting compositions (mol.%) used for phase relation experiments in this study.

	$MgSiO_3$	$Al(OH)_3$	MgO	Al_2O_3	SiO_2	H_2O	Total
A	90	10	45	2.5	45	7.5	100
B	80	20	40	5	40	15	100
C	70	30	35	7.5	35	22.5	100

in formation of hydrous phase AlOOH-$MgSiO_4H_2$ solid solution (δ-H) under the deep mantle conditions and its wide stability in the lower mantle (Suzuki et al., 2000; Ohira et al., 2014). Thus, a major water carrier in the lower mantle may be hydrous δ-H.

On the other hand, this phase coexists with $MgSiO_3$ bridgmanite, which is the major nominally anhydrous mineral of the lower mantle. Thus, the chemical reaction between bridgmanite and hydrous δ-H is an important topic to clarify the water carrier and water reservoir under lower mantle conditions. Our preliminary experiments on partitioning of aluminum between bridgmanite, its high-pressure polymorph of post-bridgmanite and hydrous phase δ-H by using the laser heated diamond anvil cell (LH-DAC) suggest its strong partitioning into hydrous phase δ-H, resulting in alumina depletion in bridgmanite and post-bridgmanite under deep lower mantle conditions (Ohira et al., 2014). However, precise partition coefficients of aluminum and also hydrogen between them have not yet been determined due to their limited grain sizes.

In this work we studied the phase relations of the $MgSiO_3$-Al_2O_3-H_2O system at high pressure and temperature by using a Kawai-type multi-anvil apparatus. Partition coefficients of aluminum and hydrogen between bridgmanite and hydrous phase δ-H at the top of the lower mantle were determined. We also determined aluminum and hydrogen partitioning between bridgmanite and hydrous phase D coexisting with hydrous phase δ-H.

2. Experimental procedure

2.1. Preparations of starting materials and the sample capsule

Starting materials are mixtures of $MgSiO_3$ enstatite and $Al(OH)_3$ gibbsite with molar ratios of $MgSiO_3$:$Al(OH)_3$ = 9:1, 8:2, and 7:3 (Table 1), each of which was prepared by mixing these compounds for 1 h. A layered starting material of $MgSiO_3$ and $Al(OH)_3$ was also employed in some runs. We used synthetic enstatite powder, which was prepared by Ishii et al. (2018a, 2019a) by the sol-gel method. Mg metal was dissolved in a solution of HNO_3 plus pure water, which was mixed with tetraethylorthosilicate $[(CH_3CH_2O)_4Si]$ at Mg/Si = 1. This solution was mixed with ammonia and stirred until it becomes gel, which was heated to 1400 °C to crystallize enstatite. A reagent grade $Al(OH)_3$ powder was dried at 150 °C before weighing. The oxide mixture and the layered samples of $MgSiO_3$ and $Al(OH)_3$ were placed in a platinum capsule with four sample rooms. The inner diameter of the sample room was 0.3 mm and the outer diameter of the capsule was 1.0 mm (Figs. 1 and 2a). The experiments of D046 and I917 adopted a single Pt-tube capsule, which was welded shut.

2.2. High pressure-temperature experiment

Phase relation experiments were conducted at 25 GPa and 28 GPa and 1000-1600 °C for 2-10 h using Kawai-type multi-anvil presses installed at the Bayerisches Geoinstitut, University of Bayreuth, Germany. Experiments at 25 GPa were performed using the 10-MN Kawai-type multi-anvil press. The pressure calibration is reported in Keppler and Frost (2005). The 15-MN Kawai-type multi-anvil press with an Osugi (DIA) guide block (IRIS-15) (Ishii et al., 2016, 2019b) was used to carry out experiments at 28 GPa. Pressures were calibrated using alumina content in bridgmanite (Liu et al., 2017a) in separate runs. Some preliminary experiments and an experiment at 28 GPa were also conducted with using the 15-MN multi-anvil press with an Osugi guide block (Discoverer-1500) installed at the Sobolev Institute of Geology and Mineralogy (Shatskiy et al., 2019). Fig. 1 shows a schematic drawing of a cell assembly used in this study. Tungsten carbide anvils with a truncated edge length of 3.0 mm was combined with a Cr-doped magnesia pressure medium with an edge length of 7 mm. A Re foil tube was used as a heater. A ZrO_2 sleeve was located around the heater for thermal insulation. Mo electrodes were put at both ends of the heater. A W-3%Re/W-25%Re thermocouple set on the surface of the central part of the heater was used for measuring sample temperature.

We increased a press load to the desired sample pressure and then temperature was increased to a target temperature. After heating for a desired duration, the sample capsule was quenched by shutting off the electric supply to the heater. Generated pressure was decreased to the atmospheric pressure in 12 hours at room temperature.

2.3. Analyses of run products

Recovered samples were mounted in epoxy resin and were polished for phase identification and textual observation by X-ray powder diffraction (XRD) and scanning electron microscopy, respectively. A LEO1530 scanning electron microscope with an energy-dispersive X-ray spectrometer was operated at an acceleration voltage of 10-15 kV and a beam current of 10 nA. Composition analysis of phases in quench run products were performed using a JEOL JXA-8200 electron probe microanalyzer (EPMA) operating at an acceleration voltage of 10 kV and a beam current of 5 nA with a standard of pyrope for Mg, Si, and Al. XRD measurements of run products were conducted using a micro-focus X-ray diffractometer (Bruker, D8 DISCOVER) equipped with a two-dimensional solid-state detector (VÅNTEC500) and a micro-focus source (IμS) with Co-Kα radiation operated at 40 kV and 500 μA.

Water contents of phases in two layered samples (I682 and I691) were determined by the Fourier transformation infrared spectroscopy (FTIR) using a Bruker IFS 120 high-resolution spectrometer coupled with a Bruker IR microscope. Before the measurement, both sides of the recovered samples were polished to a thickness of 50 μm. An aperture size of 20 μm was adopted for the measurements.

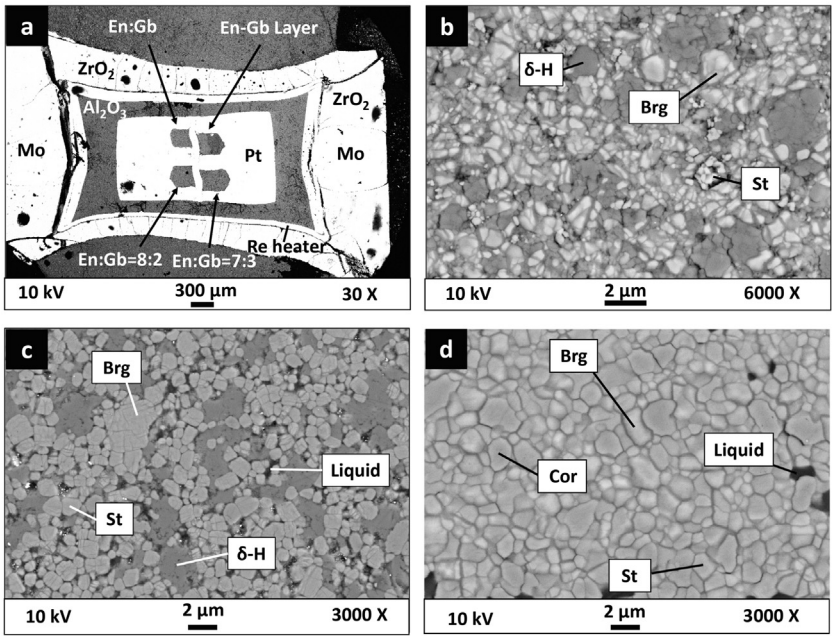

Fig. 2. Representative BSE images of the recovered samples at 28 GPa. (a) The example of polished capsule at 1400 °C. (b), (c) and (d) En:Gb=8:2 at 1000 °C, 1300 °C, and (d) 1600 °C, respectively. Brg, bridgmanite; δ-H, hydrous phase δ-H; D, hydrous phase D; St, stishovite.

Table 2
Experimental conditions and run products.

Run No.	S.M.†	P (GPa)	T (°C)	D (h)	Run products	$D_{Al}(\delta/Brg)$
S7167	B	25	1000	10	Brg+δ-H+D+St	180(50)
S7169	B	25	1200	4	Brg+δ-H+St+L	54(14)
S7149	B	25	1400	3	Brg+St+Cor+L	–
I685	A	28	1000	10	Brg+D+δ-H+St	119(35)
	B	28	1000	10	Brg+D+δ-H+St	143(80)
	C	28	1000	10	Brg+D+δ-H+St	153(98)
	En-Gb layer	28	1000	10	Brg/D/δ-H	–
D046¶	En-Gb layer	28	1100	3	Brg/D/δ-H	–
I682	A	28	1100	6	Brg+D+δ-H+St	68(35)
	B	28	1100	6	Brg+D+δ-H+St	75(35)
	C	28	1100	6	Brg+D+δ-H+St	82(42)
	En-Gb layer	28	1100	6	Brg/D/δ-H	–
I1034	A	28	1300	6	Brg+δ-H+St+L	43(8)
	B	28	1300	6	Brg+δ-H+St+L	42(9)
	C	28	1300	6	Brg+δ-H+St+L	50(6)
I691	A	28	1400	3	Brg+δ-H(tr)+Cor(tr)+St+L	–
	B	28	1400	3	Brg+δ-H(tr)+Cor+St+L	–
	C	28	1400	3	Brg+δ-H(tr)+Cor+St+L	–
	En-Gb layer	28	1400	3	Brg/δ-H/Cor	–
I917	B	28	1500*	4	Brg+St+Cor+L	–
I694	A	28	1600	2	Brg+St+L	–
	B	28	1600	2	Brg+St+Cor+L	–
	C	28	1600	2	Brg+St+Cor+L	-
	En-Gb layer	28	1600	2	Brg+St+Cor+L	–

Brg, bridgmanite; δ-H, hydrous phase δ-H; D, hydrous phase D; St, stishovite; Cor, corundum, L, liquid; S.M., starting material; tr, trace.
† See Table 1.
*Temperature was kept around 1500-1520 °C.
¶This experiment was performed with Discoverer-1500 (see text).

3. Results and discussion

3.1. Phase relations of $MgSiO_3$-Al_2O_3-H_2O system at the top of the lower mantle

The experimental conditions and run products are summarized in Table 2. Representative back-scattered electron (BSE) images of polished samples are given in Fig. 2. BSE images of the layered samples recovered from 1100 °C and 1400 °C at 28 GPa (I682 and I691, respectively) are shown in Fig. 3a and b, respectively. Fig. 4 shows a compositional profile in the layered sample synthesized at 28 GPa and 1100 °C (D046). Compositions of the recovered phases are summarized in Table S1. Typical XRD patterns of the run products are given in Fig. 5, which indicates coexistence of bridgmanite and hydrous phase δ-H at 1100 °C and disappearance of phase δ-H at 1600 °C at 28 GPa.

The phase relations of $MgSiO_3$-Al_2O_3-H_2O system are shown in Fig. 6. Although we used different bulk compositions with different ratios of $MgSiO_3$ and $Al(OH)_3$ (Table 1), the phase assemblages in the run products at the same pressure and temperature

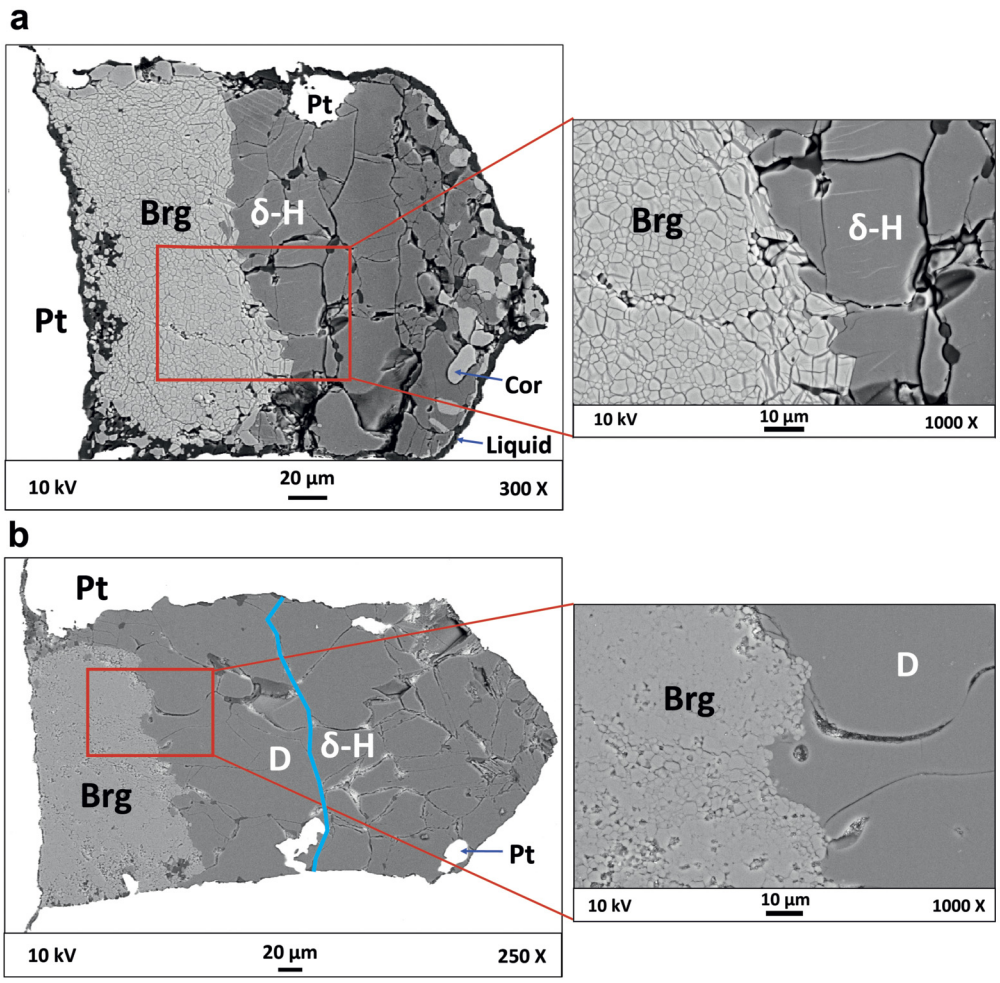

Fig. 3. The BSE images of the layered samples of (a) bridgmanite and hydrous phase δ recovered from 28 GPa and 1400 °C (I691), (b) bridgmanite and hydrous phases D and δ recovered from 28 GPa and 1100 °C (I682). Brg, bridgmanite; δ-H, hydrous phase δ-H; D, hydrous phase D; Cor, corundum.

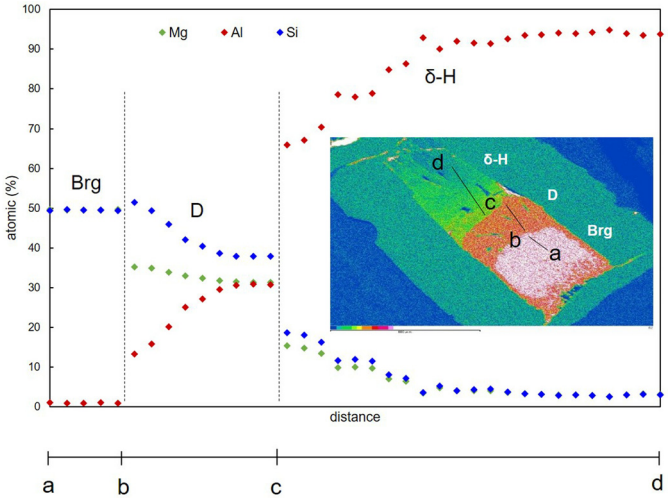

Fig. 4. The compositional profile across the sample recovered from 28 GPa and 1100 °C (D046) from bridgmanite to hydrous phase δ-H solid solution through hydrous phase D. Brg, bridgmanite; δ-H, phase δ-H; D, phase D; Cor, corundum. Coupled changes of Mg, Si in δ-H phase indicate the substitution of $2Al^{3+} = Mg^{2+} + Si^{4+}$. Decoupled relations between Mg and Si contents in phase D suggest that the main substitution mechanism might be $H^{+} + Al^{3+} = Si^{4+}$. Brg, bridgmanite; δ-H, hydrous phase δ-H; D, hydrous phase D; Cor, corundum.

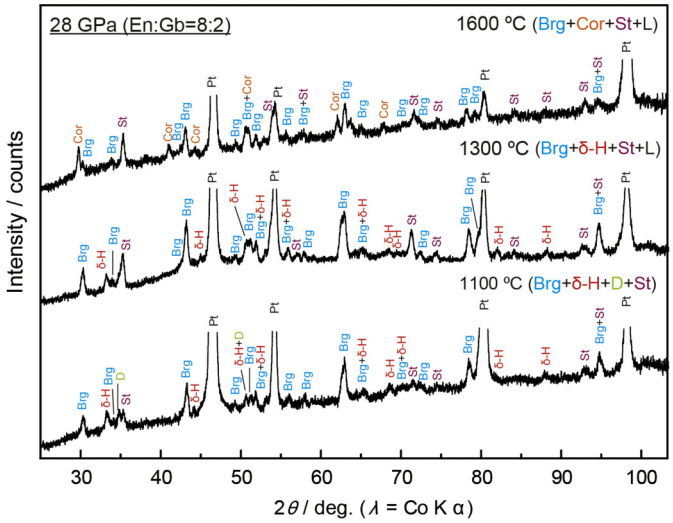

Fig. 5. Representative X-ray diffraction patterns of the run products recovered from 28 GPa and 1100, 1300, and 1600 °C. Brg, bridgmanite; δ-H, hydrous phase δ-H; D, hydrous phase D; Cor, corundum.

were the same (Table 2). Hydrous phases D and δ-H are stable below 1100 °C and up to 1400 °C, respectively, coexisting with Al-poor bridgmanite, at 25-28 GPa. At higher temperatures, no hydrous phases are stable and Al-rich bridgmanite ± corundum appears instead. Note that hydrous phase D was not distinguished by BSE images in run products from the mixture starting sam-

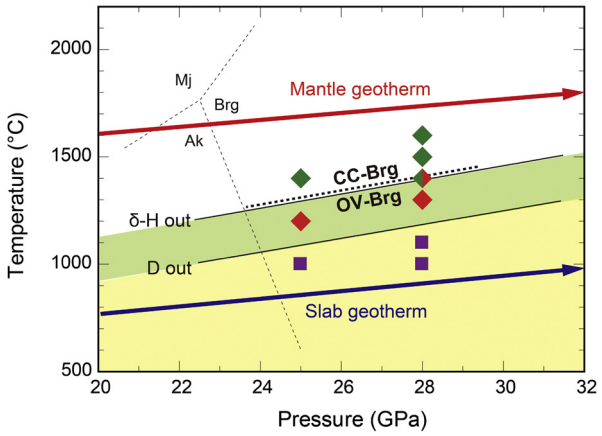

Fig. 6. Phase relations in $MgSiO_3$-$Al(OH)_3$ system determined in this study. Purple squares are bridgmanite (Brg) + hydrous phase δ-H (δ-H) + hydrous phase D (D) + stishovite. Red diamonds are Brg + δ-H + stishovite + liquid. Green diamonds are Brg ± corundum + stishovite + liquid. Thin solid lines are disappearance boundaries of D and δ-H (D out and δ-H out, respectively). The bold dashed line is a boundary between bridgmanites with $MgAlO_{2.5}$ oxygen vacancy (OV) and Al_2O_3 charge-coupling (CC), which is defined by alumina content in bridgmanite reported in previous studies (Kojitani et al., 2007; Liu et al. 2017b; see the text). The thin dashed lines are phase boundaries in $MgSiO_3$ system (Ishii et al., 2011). Mj, $MgSiO_3$ majorite; Ak, $MgSiO_3$ akimotoite. (For interpretation of the colors in the figure(s), the reader is referred to the web version of this article.)

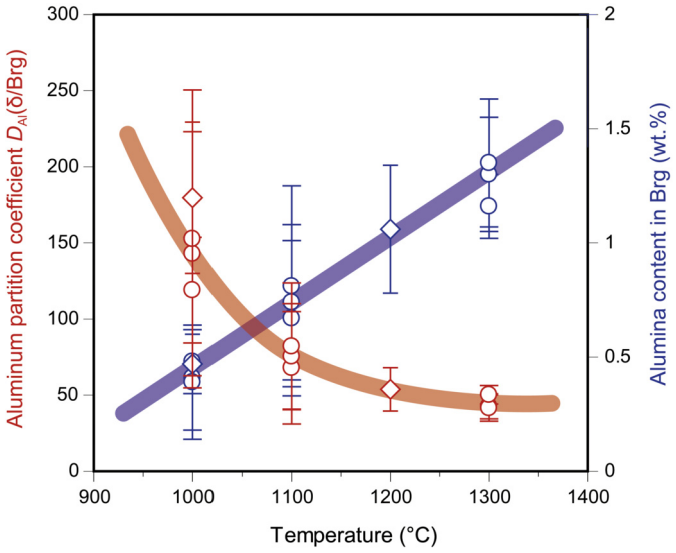

Fig. 7. Aluminum partition coefficient between hydrous phase δ-H and bridgmanite and alumina content in bridgmanite coexisting with hydrous phase δ-H at 25 and 28 GPa and various temperatures. A blue line and markers (circles for 28 GPa and diamonds for 25 GPa) indicate the temperature change in alumina contents in bridgmanite, and a red line and markers (circles for 28 GPa and diamonds for 25 GPa) are the temperature change of the aluminum partition coefficients.

ples but was identified by XRD profiles (Fig. 5). Small amounts of stishovite appeared in all runs above 1000 °C. The composition of phase δ-H at 25 GPa and 1000 °C is 99 mol.%$Al_2O_2(OH)_2$ −1 mol.%$MgSiO_2(OH)_2$, whereas those at 25 GPa and 1200 °C and 28 GPa and 1000 °C are 73 mol.%$Al_2O_2(OH)_2$ −27 mol.%$MgSiO_2(OH)_2$ and 75∼77 mol.%$Al_2O_2(OH)_2$ −23∼25 mol.%$MgSiO_2(OH)_2$, respectively. An LH-DAC study by Ohira et al. (2014) reported the composition of hydrous phase δ-H is 57 mol.%$Al_2O_2(OH)_2$ −43 mol.%$MgSiO_2(OH)_2$ at 68 GPa and 1700 °C. These results imply strong temperature and pressure dependence on solubility of the phase H component. At 28 GPa and 1300 °C, an excess SiO_2 component was observed showing 61∼62mol%$Al_2O_2(OH)_2$ −26∼28 mol%$MgSiO_2(OH)_2$ −11∼12 mol%SiO_2. At the temperatures above dehydration of hydrous phase D, Mg-rich hydrous liquid was identified by the compositional measurements based on loss of the analysis total (∼50 wt.%), although its composition was not precise enough due to the small size and small fraction of the quench hydrous liquid. The present phase relations indicate that hydrous phase D is stable along the cold slab geotherm (e.g. Thompson, 1992), whereas hydrous phase δ-H is stable up to higher temperatures but lower than the average mantle geotherm (Akaogi et al., 1989).

3.2. Partitioning of aluminum between bridgmanite and hydrous phase δ-H, and bridgmanite and hydrous phase D

At 25-28 GPa, the alumina contents of bridgmanite increase with increasing temperature (Table S1 and Fig. 7). When bridgmanite coexists with hydrous phase δ-H ± D, alumina contents in bridgmanite are 0.41-3.82 wt.% at 1000-1400 °C. Alumina contents in bridgmanite without hydrous phases at higher temperatures are higher than 5 wt.%. Thus, bridgmanite coexisting with the hydrous phases δ-H ± D is significantly depleted in alumina. The partition coefficient of aluminum D_{Al}(δ-H/Brg), which was calculated using Al_2O_3 content in wt.%, between hydrous phase δ-H and bridgmanite is very large around 42∼180 at the top of the lower mantle at 25-28 GPa, which decreases with increasing temperature (Fig. 7). Ohira et al. (2014) determined that D_{Al}(δ-H/Brg) is 13 at 68 GPa and 1700 °C, whereas D_{Al}(δ-H/post-bridgmanite) is 8 at 128 GPa and 1600 °C, by transmission electron microscopic analysis in combination with energy-dispersive X-ray spectroscopy of the recovered samples from the LH-DAC experiments. Thus, D_{Al} may significantly decrease with increasing temperature also at higher pressures, although there is a possibility that the difference is due to analytical errors in DAC samples. In the samples recovered from the DAC experiments, the grain sizes of bridgmanite and hydrous phase δ-H were very small (<100 nm). Therefore, it is likely that overlapping of the two grains produced relatively high alumina content in bridgmanite, resulting in the smaller partition coefficients. Further study by multi-anvil experiments at higher pressures is needed to clarify D_{Al} under deep lower mantle conditions.

We also examined aluminum partitioning between bridgmanite and hydrous phase D using the layered sample (D046) because hydrous phase D grains of the mixture samples could not be analyzed by EPMA due to undistinguishable BSE images of phase D as mentioned above (section 3.1). Alumina is also enriched in hydrous phase D and depleted in bridgmanite (<1 wt.%). The D_{Al}(D/Brg) using grains near the bridgmanite-hydrous phase D grain boundary is ∼10, which is smaller than that between hydrous phase δ-H solid solution and bridgmanite (Fig. 4).

Litasov and Ohtani (2003) reported Al partitioning between bridgmanite and superhydrous phase B, showing Al depletion in bridgmanite (0.76-1.32 wt.%) when coexisting with superhydrous phase B (up to 4.72 wt.%), in hydrous peridotite of the MgO-SiO_2-Al_2O_3-CaO-H_2O system. Thus, major hydrous phases in the lower mantle generally have a capability of reducing alumina in bridgmanite.

3.3. Partitioning of hydrogen between bridgmanite and hydrous phases

Water contents in bridgmanite coexisting with hydrous phases δ-H and D were analyzed by using micro-FTIR measurement. We measured FTIR spectra for the polycrystalline bridgmanites with layered configurations of bridgmanite/phase δ-H and bridgmanite/phase D/phase δ-H, in which the grain sizes of bridgmanite were around 1-3 μm (Fig. 8). The water contents of the both-side polished samples were measured at regions very close to the boundary with hydrous phase δ-H or phase D (as close as 20 μm) and the center of the bridgmanite layer (about 60 μm apart from

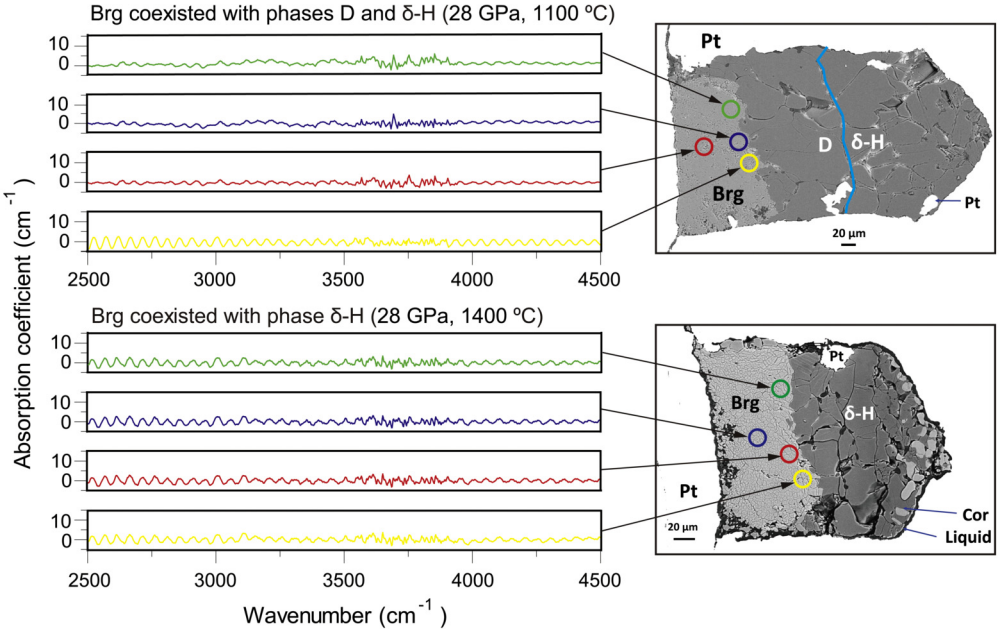

Fig. 8. Representative FTIR spectra from bridgmanite polycrystals coexisting with hydrous phases D and δ-H measured near the boundaries between bridgmanite and hydrous phase D or δ-H. The circles are measured areas within ~20 and ~60 μm apart from the boundary of hydrous phase D and δ-H layers. The colors of the circles correspond to those of FTIR spectra.

the boundary). FTIR spectra from bridgmanite grains show no detectable peaks corresponding to the OH vibration. The water content in bridgmanite is thus negligible less than 1 ppm, i.e., water is stored in hydrous phase δ-H or D, and coexisting bridgmanite is essentially dry at least at the top of the lower mantle. The strong hydrogen partitioning into the hydrous phase A was also shown in those of olivine and wadsleyite (Ishii and Ohtani, 2021), implying that such strong hydrogen partitioning into hydrous phases is a common phenomenon. Bridgmanite containing Al_2O_3 less than 5 wt.% has the oxygen vacancy component of $MgAlO_{2.5}$, whereas that containing higher Al_2O_3 has only the charge-coupled component of Al_2O_3 (Kojitani et al., 2007; Liu et al., 2017b). The present results on bridgmanite compositions are consistent with this observation, i.e., bridgmanites coexisting with the hydrous phases δ-H and D have low Al_2O_3 contents less than 5 wt.% having the oxygen vacancy component of $MgAlO_{2.5}$, whereas bridgmanite has only the charge-coupled component of Al_2O_3 out of the stability field of hydrous phases δ-H and D (Fig. 6). Navrotsky (1999) suggested that oxygen vacancies may incorporate water into bridgmanite (V_o+O_2 + H_2O = $2OH^-$). Our results clearly indicate that this hypothesis is not applicable at least when the hydrous phases coexist with bridgmanite due to strong hydrogen partitioning to hydrous phases δ-H and D.

3.4. Geochemical implications

Our results show strong aluminum and hydrogen partitioning into hydrous phases δ-H and D. Phase δ-H exists at the lower mantle pressure and low temperatures in hydrous peridotite and basalt systems (Ohira et al., 2016; Ohira, 2018). Fluids dehydrated at the top of the lower mantle may react with aluminous bridgmanite along the geotherms of the slabs to create alumina-depleted bridgmanite coexisting with hydrous phase δ-H ± phase D. Alumina contents of bridgmanite in dry MORB and peridotite are ~15 wt.% and ~5 wt.% (Litasov and Ohtani, 2005; Litasov et al., 2005; Ishii et al., 2011, 2018b, 2019c), respectively. Based on D_{Al}(δ-H/Brg) determined in this study, their alumina contents decrease significantly to less than ~6 wt.% and ~1 wt.%, respectively, by the reaction with water and the subsequent formation of hydrous phase δ-H. Depletion of alumina in bridgmanite under the wet conditions coexisting with hydrous phase δ-H provides significant effects on mantle dynamics due to modification of the phase relations, i.e., the alumina depletion may cause slab subduction further into the deep lower mantle since the garnet–bridgmanite phase boundary becomes shallower and the wet slab thus becomes denser than the dry surrounding mantle at low temperature coexisting with hydrous phases. The depletion of alumina also lowers the post-bridgmanite transition pressure and sharpens the phase transition at the base of the lower mantle (Tateno et al., 2005; Hirose et al., 2006). The post-bridgmanite phase boundary under the wet condition coexisting with hydrous phase δ-H is consistent with the D" layer pressure reported in seismology. Grocholski et al. (2012) reported that the phase boundary of the dry post-bridgmanite transition in peridotite locates at a depth greater than that of the D" layer, i.e., the post-bridgmanite transition pressure is not consistent with the D" discontinuity pressure, although the phase transition pressures for the alumina-free forsterite and San Carlos olivine composition are consistent with the D" discontinuity pressure. On the other hand, the post-bridgmanite phase transition under the wet conditions coexisting with hydrous phase δ-H provides sharp and shallower phase boundary based on the phase relations of MgO-Al_2O_3-SiO_2-H_2O and MgO-Fe_2O_3-Al_2O_3-SiO_2-H_2O systems (Ohira et al., 2014; Yuan et al., 2019; Ohtani, 2021). The results in these previous studies are in good agreement with our observations of bridgmanite chemistry coexisting with the hydrous phases under the wet conditions.

The present study shows that the water content in bridgmanite coexisting with hydrous phase δ-H and/or hydrous phase D is very low, less than 1 ppm (Fig. 8). This extremely dry composition of bridgmanite is consistent with the water content in bridgmanite coexisting with superhydrous phase B (Bolfan-Casanova et al., 2003). These results indicate that the water carriers in MORB and peridotite layers of the slabs are hydrous phase δ-H, phase D, or superhydrous phase B, and bridgmanite is not the water carrier at least in the uppermost lower mantle. Dry bridgmanite coexisting with hydrous phases under lower mantle conditions could provide the dry deformation and rheology of the wet slabs in the lower mantle.

4. Conclusion

Our phase relation experiments in $MgSiO_3$-Al_2O_3-H_2O system revealed that both of hydrous phases D and δ-H coexist with bridgmanite at 25-28 GPa and 1000-1100 °C, whereas only hydrous phase δ-H coexists above 1200 °C at the same pressure range. Aluminum strongly partitions to hydrous phase δ-H, resulting in strong depletion in alumina in bridgmanite. The depletion of alumina in bridgmanite modifies the phase relations significantly in the lower mantle, i.e., both the pressures of the garnet-bridgmanite and post-bridgmanite transformations are reduced under the wet conditions. The pressure decrease of the garnet-bridgmanite transition in MORB and peridotite under wet conditions facilitates subduction of wet slabs into the deep lower mantle. The post-bridgmanite phase boundary under the wet condition is consistent with the D" layer pressure reported in seismology when bridgmanite has a very low alumina content around one percent or less. We confirmed by FTIR measurement that bridgmanite coexisting with hydrous phase δ-H, and/or phase D is dry. Bridgmanite coexisting with superhydrous phase B is also dry (Bolfan-Casanova et al., 2003). Thus, the dry nature of bridgmanite coexisting with hydrous phases indicate that the major water carriers in the lower mantle are high-pressure hydrous phases such as phase δ-H, phase D, and superhydrous phase B. Bridgmanite is not a water reservoir at least at the top of the lower mantle, and provides dry deformation and rheology of the wet slabs in the lower mantle.

CRediT authorship contribution statement

Takayuki Ishii: Conceptualization, Formal analysis, Funding acquisition, Investigation, Methodology, Project administration, Validation, Visualization, Writing – original draft. **Eiji Ohtani:** Conceptualization, Funding acquisition, Methodology, Writing – original draft. **Anton Shatskiy:** Investigation, Writing – review & editing.

Declaration of competing interest

The authors declare that they have no competing interests or personal relationships that could have appeared to influence the work reported in this paper.

Acknowledgement

We thank R. Njul for preparation of thin-section samples, L. Yuan for the chemical composition analysis of the D046 sample, H. Keppler for help and advice in measurements of water contents in the samples by using FTIR, and T. Katsura and D. J. Frost for useful discussion. We also thank two anonymous reviewers for their fruitful comments. This work was supported by the Grants-in-Aid of the German Research Foundation (no. IS350/1-1 for T.I.). E.O. was supported by the KAKENHI Grant Number JP15H05748 and JP20H00187, and by the research award from the Alexander von Humboldt Foundation. A.S. was supported by RFBR No. 21-55-14001 and the state assignment of IGM RAS.

Appendix A. Supplementary material

Supplementary material related to this article can be found online at https://doi.org/10.1016/j.epsl.2022.117441.

References

Akaogi, M., Ito, E., Navrotsky, A., 1989. Olivine-modified spinel-spinel transitions in the system Mg_2SiO_4-Fe_2SiO_4: calorimetric measurements, thermochemical calculation, and geophysical application. J. Geophys. Res., Solid Earth 94, 15671–15685.

Bindi, L., Nishi, M., Tsuchiya, J., Irifune, T., 2014. Crystal chemistry of dense hydrous magnesium silicates: the structure of phase H, $MgSiH_2O_4$, synthesized at 45 GPa and 1000 °C. Am. Mineral. 99, 1802–1805.

Bolfan-Casanova, N., Keppler, H., Rubie, D.C., 2003. Water partitioning at 660 km depth and evidence for very low water solubility in magnesium silicate perovskite. Geophys. Res. Lett. 30, 1905.

Duan, Y., Sun, N., Wang, S., Li, X., Guo, X., Ni, H., Prakapenka, V.B., Mao, Z., 2018. Phase stability and thermal equation of state of δ-AlOOH: implication for water transportation to the deep lower mantle. Earth Planet. Sci. Lett. 494, 92–98.

Fei, H., Yamazaki, D., Sakurai, M., Miyajima, N., Ohfuji, H., Katsura, T., Yamamoto, T., 2017. A nearly water-saturated mantle transition zone inferred from mineral viscosity. Sci. Adv. 3, e1603024.

Freitas, D., Manthilake, G., Schiavi, F., Chantel, J., Bolfan-Casanova, N., Bouhifd, M.A., Andrault, D., 2017. Experimental evidence supporting a global melt layer at the base of the Earth's upper mantle. Nat. Commun. 8, 1–7.

Fukao, Y., Obayashi, M., 2013. Subducted slabs stagnant above, penetrating through, and trapped below the 660 km discontinuity. J. Geophys. Res., Solid Earth 118, 5920–5938.

Grocholski, B., Catalli, K., Shim, S., Prakapenka, V., 2012. Mineralogical effects on the detectability of the postperovskite boundary. Proc. Natl. Acad. Sci. USA 109, 2275–2279.

Hirose, K., Sinmyo, R., Sata, N., Ohishi, Y., 2006. Determination of post-perovskite phase transition boundary in $MgSiO_3$ using Au and MgO pressure standards. Geophys. Res. Lett. 33, L013010.

Hsieh, W.P., Ishii, T., Chao, K.H., Tsuchiya, J., Deschamps, F., Ohtani, E., 2020. Spin transition of iron in δ-(Al, Fe) OOH induces thermal anomalies in Earth's lower mantle. Geophys. Res. Lett. 47, e2020GL087036.

Ishii, T., Kojitani, H., Akaogi, M., 2011. Post-spinel transitions in pyrolite and Mg_2SiO_4 and akimotoite–perovskite transition in $MgSiO_3$: precise comparison by high-pressure high-temperature experiments with multi-sample cell technique. Earth Planet. Sci. Lett. 309, 185–197.

Ishii, T., Shi, L., Huang, R., Tsujino, N., Druzhbin, D., Myhill, R., Li, Y., Wang, l., Yamamoto, T., Miyajima, N., Kawazoe, T., Nishiyama, N., Higo, Y., Tange, Y., Katsura, T., 2016. Generation of pressure over 40 GPa using Kawai–type multi–anvil press with tungsten carbide anvils. Rev. Sci. Instrum. 87, 024501-1–024501-6.

Ishii, T., Huang, R., Fei, H., Koemets, I., Liu, Z., Maeda, F., Yuan, L., Wang, L., Druzhbin, D., Yamamoto, T., 2018a. Complete agreement of the post-spinel transition with the 660-km seismic discontinuity. Sci. Rep. 8, 1–6.

Ishii, T., Kojitani, H., Akaogi, M., 2018b. Phase relations and mineral chemistry in pyrolitic mantle at 1600–2200 °C under pressures up to the uppermost lower mantle: phase transitions around the 660-km discontinuity and dynamics of upwelling hot plumes. Phys. Earth Planet. Inter. 274, 127–137.

Ishii, T., Huang, R., Myhill, R., Fei, H., Koemets, I., Liu, Z., Maeda, F., Yuan, L., Wang, L., Druzhbin, D., 2019a. Sharp 660-km discontinuity controlled by extremely narrow binary post-spinel transition. Nat. Geosci. 12, 869–872.

Ishii, T., Liu, Z., Katsura, T., 2019b. A breakthrough in pressure generation by a Kawai-type multi-anvil apparatus with tungsten carbide anvils. Engineering 5, 434–440.

Ishii, T., Kojitani, H., Akaogi, M., 2019c. Phase relations of harzburgite and MORB up to the uppermost lower mantle conditions: precise comparison with pyrolite by multisample cell high-pressure experiments with implication to dynamics of subducted slabs. J. Geophys. Res., Solid Earth 124, 3491–3507.

Ishii, T., Ohtani, E., 2021. Dry metastable olivine and slab deformation in a wet subducting slab. Nat. Geosci. 14, 526–530.

Karato, S., 2011. Water distribution across the mantle transition zone and its implications for global material circulation. Earth Planet. Sci. Lett. 301, 413–423.

Keppler, H., Frost, D., 2005. In: Miletich, R. (Ed.), Mineral Behavior at Extreme Conditions. In: EMU Notes in Mineralogy, vol. 7, pp. 1–30. Chap. 1.

Kojitani, H., Katsura, T., Akaogi, M., 2007. Aluminum substitution mechanisms in perovskite-type $MgSiO_3$: an investigation by Rietveld analysis. Phys. Chem. Miner. 34, 257–267.

Lawrence, J.F., Wysession, M.E., 2006. Seismic evidence for subduction-transported water in the lower mantle. In: Geophys. Monogr. Ser., vol. 168, pp. 251–261.

Litasov, K., Ohtani, E., 2003. Stability of various hydrous phases in CMAS pyrolite-H_2O system up to 25 GPa. Phys. Chem. Miner. 30, 147–156.

Litasov, K.D., Ohtani, E., 2005. Phase relations in hydrous MORB at 18–28 GPa: implications for heterogeneity of the lower mantle. Phys. Earth Planet. Inter. 150, 239–263.

Litasov, K., Ohtani, E., Sano, A., Suzuki, A., Funakoshi, K., 2005. In situ X-ray diffraction study of post-spinel transformation in a peridotite mantle: implication for the 660-km discontinuity. Earth Planet. Sci. Lett. 238, 311–328.

Liu, Z., Nishi, M., Ishii, T., Fei, H., Miyajima, N., Ballaran, T.B., Ohfuji, H., Sakai, T., Wang, L., Shcheka, S., Arimoto, T., Tange, Y., Higo, Y., Irifune, T., Katsura, T., 2017a. Phase relations in the system $MgSiO_3$-Al_2O_3 up to 2300 K at lower mantle pressures. J. Geophys. Res., Solid Earth 122, 7775–7788.

Liu, Z., Ishii, T., Katsura, T., 2017b. Rapid decrease of $MgAlO_{2.5}$ component in bridgmanite with pressure. Geochem. Perspect. Lett. 5, 12–18.

Navrotsky, A., 1999. A lesson from ceramics. Science 284, 1788–1789.

Nishi, M., Irifune, T., Tsuchiya, J., Tange, Y., Nishihara, Y., Fujino, K., Higo, Y., 2014. Stability of hydrous silicate at high pressures and water transport to the deep lower mantle. Nat. Geosci. 7, 224–227.

Ohira, I., Ohtani, E., Kamada, S., Hirao, N., 2016. Formation of phase H-δ-AlOOH solid solution in the lower mantle. In: Goldschmidt Conference Abstract, p. 2346.

Ohira, I., Ohtani, E., Sakai, T., Miyahara, M., Hirao, N., Ohishi, Y., Nishijima, M., 2014. Stability of a hydrous δ-phase, AlOOH–$MgSiO_2(OH)_2$, and a mechanism for water transport into the base of lower mantle. Earth Planet. Sci. Lett. 401, 12–17.

Ohira, I., 2018. Phase equilibrium experiments assessing the stability of δ-AlOOH–ε-FeOOH–$MgSiO_4H_2$ Phase H solid solutions. In: Experimental Study of δ-AlOOH–ε-FeOOH–Phase H Solid Solution Toward Understanding the Water Transport and Seismic Anomaly in the Earth's Lower Mantle. Tohoku University, Sendai, Japan, pp. 16–50. chapter 2, Ph. D. thesis.

Ohtani, E., 2005. Water in the mantle. Elements 1, 25–30.

Ohtani, E., Amaike, Y., Kamada, S., Sakamaki, T., Hirao, N., 2014. Stability of hydrous phase H $MgSiO_4H_2$ under lower mantle conditions. Geophys. Res. Lett. 41, 8283–8287.

Ohtani, E., 2021. Hydration and dehydration in Earth's interior. Annu. Rev. Earth Planet. Sci. 49, 253–278.

Pearson, D.G., Brenker, F.E., Nestola, F., McNeill, J., Nasdala, L., Hutchison, M.T., Matveev, S., Mather, K., Silversmit, G., Schmitz, S., Vekemans, B., Vincze, L., 2014. Hydrous mantle transition zone indicated by ringwoodite included within diamond. Nature 507, 221–224.

Sano, A., Ohtani, E., Kondo, T., Hirao, N., Sakai, T., Sata, N., Ohishi, Y., Kikegawa, T., 2008. Aluminous hydrous mineral δ-AlOOH as a carrier of hydrogen into the core-mantle boundary. Geophys. Res. Lett. 35, 1–5.

Sano-Furukawa, A., Hattori, T., Komatsu, K., Kagi, H., Nagai, T., Molaison, J.J., dos Santos, A.M., Christopher, A., 2018. Tulk direct observation of symmetrization of hydrogen bond in δ-AlOOH under mantle conditions using neutron diffraction. Sci. Rep. 8, 1–9.

Satta, N., Criniti, G., Kurnosov, A., Boffa Ballaran, T., Ishii, T., Marquardt, H., 2021. High-pressure elasticity of δ-(Al, Fe) OOH single crystals and seismic detectability of hydrous MORB in the shallow lower mantle. Geophys. Res. Lett. 48, e2021GL094185.

Schmandt, B., Jacobsen, S.D., Becker, T.W., Liu, Z., Ducker, K.G., 2014. Dehydration melting at the top of the lower mantle. Science 344, 1265–1268.

Shatskiy, A., Arefiev, A.V., Podborodnikov, I.V., Litasov, K.D., 2019. Origin of K-rich diamond-forming immiscible melts and CO_2 fluid via partial melting of carbonated pelites at a depth of 180–200 km. Gondwana Res. 75, 154–171.

Suzuki, A., Ohtani, E., Kamada, T., 2000. A new hydrous phase δ-AlOOH synthesized at 21 GPa and 1000 °C. Phys. Chem. Miner. 27, 689–693.

Tateno, S., Hirose, K., Sata, N., Ohishi, Y., 2005. Phase relations in $Mg_3Al_2Si_3O_{12}$ to 180 GPa: effect of Al on post-perovskite phase transition. Geophys. Res. Lett. 32, L15306.

Thompson, A.B., 1992. Water in the Earth's upper mantle. Nature 358, 295–302.

Tschauner, O., Huang, S., Greenberg, E., Prakapenka, V., Ma, C., Rossman, G.R., Shen, A.H., Zhang, D., Newville, M., Lanzirotti, A., Tait, K., 2018. Ice-VII inclusions in diamonds: evidence for aqueous fluid in Earth's deep mantle. Science 359, 1136–1139.

Utada, H., Koyama, T., Obayashi, M., Fukao, Y., 2009. A joint interpretation of electromagnetic and seismic tomography models suggests the mantle transition zone below Europe is dry. Earth Planet. Sci. Lett. 281, 249–257.

Wang, F., Barklage, M., Lou, X., van der Lee, S., Bina, C.R., Jacobsen, S.D., 2018. HyMaTZ: a Python program for modeling seismic velocities in hydrous regions of the mantle transition zone. Geochem. Geophys. Geosyst. 19, 2308–2324.

Wirth, R., Vollmer, C., Brenker, F., Matsyuk, S., Kaminsky, F., 2007. Inclusions of nanocrystalline hydrous aluminium silicate "Phase Egg" in superdeep diamonds from Juina (Mato Grosso State, Brazil). Earth Planet. Sci. Lett. 259, 384–399.

Yoshino, T., Katsura, T., 2013. Electrical conductivity of mantle minerals: role of water in conductivity anomalies. Annu. Rev. Earth Planet. Sci. 41, 605–628.

Yuan, H., Zhang, L., Ohtani, E., Meng, Y., Greenberg, E., Prakapenka, V.B., 2019. Stability of Fe-bearing hydrous phases and element partitioning in the system MgO–Al_2O_3–Fe_2O_3–SiO_2–H_2O in Earth's lowermost mantle. Earth Planet. Sci. Lett. 524, 115714.